JMEPEG (2012) 21:1645–1654
DOI: 10.1007/s11665-011-0074-2

1059-9495/$19.00

Influence of Processing Parameters on Induced Energy, Mechanical and Corrosion Properties of FSW Butt Joint of 7475 AA

Rajesh Kumar Gupta, Hrishikesh Das, and Tapan Kumar Pal

(Submitted July 5, 2011; in revised form September 29, 2011)

Friction stir welding (FSW), a promising solid state joining process invented at TWI in 1991, was used to join 9 mm thick 7475 aluminum alloy which is considered essentially unweldable by fusion processes. In the present work, the process parameters such as tool rotational speed were varied from 300 to 1000 rpm for a travel speed of 50 mm/min and the influence of process parameters in terms of energy input on microstructure, hardness, tensile strength, and the corrosion property of 7475 aluminum joints was evaluated and analyzed. The maximum tensile strength of FSW joints was obtained at rotational speed of 400 rpm and traverse speed of 50 mm/min (59.2 kJ) which attributed maximum stirred zone area and maximum hardness. The maximum corrosion resistance properties of weld in 3.5% NaCl solution, however, were obtained at rotational speed of 1000 rpm and traverse speed of 50 mm/min. Furthermore, for a given weld, stirred zone showed improved corrosion properties than TMAZ.

Keywords energy and corrosion rate, friction stir welding (FSW), stir zone (SZ), thermo mechanically affected zone (TMAZ)

1. Introduction

Friction stir welding (FSW) is an innovative welding process developed by the welding institute (TWI), Cambridge, UK, in 1991 (Ref 1). This process has emerged as a new solid state joining technique, especially for high strength aluminum alloys that are difficult to weld using conventional fusion technique. To accomplish a FSW, a rotating tool is forced into the material and traversed along the joint under appropriate conditions. Friction between the tool and the workpiece results in localized heating which raises the temperature of the material to the range where it is plastically deformed. A welded joint is produced as a result of this localized heating and complex movement of the metal around the pin. The determination of optimum FSW conditions is very important to obtain sound joint as well as the required joint properties.

The FSW process generates three distinct microstructural zones: stirred zone (SZ), thermo mechanically affected zone (TMAZ), and heat-affected zone (HAZ). Because the production of the three zones, particularly SZ of fine grained structure, significantly affects the mechanical properties, understanding the evaluation of the FSW microstructure is of significant technological and scientific interest.

Rajesh Kumar Gupta, Hrishikesh Das, and **Tapan Kumar Pal**, Welding Technology Centre, Metallurgical and Material Engineering Department, Jadavpur University, Kolkata 700032, India. Contact e-mails: talktorajeshgupta@gmail.com, hrishichem@gmail.com, and tkpal.ju@gmail.com.

There have been a number of reports (Ref 2-16) highlighting the microstructural changes due to plastic deformation and frictional heat associated with FSW. Mechanical failure of the welds can take place in the SZ, TMAZ, or HAZ region depending on the amount of energy input which is controlled by the welding parameters such as rotational and travel speed (Ref 3-12). Since the material flow behavior is predominantly influenced by the material properties such as yield strength, ductility and hardness of the base metal, tool design (Ref 17), and FSW process parameters, the dependence of weld microstructure on process parameters differs in different aluminum alloys for a given tool design.

The changes in the microstructure are associated not only with mechanical properties but also with the corrosion properties of the welds as well. The corrosion properties of the FSW in different aluminum alloys have been examined by a number of authors (Ref 18-26). Corrosion attack has been found in SZ, at the interface between the SZ and TMAZ (Ref 19) and also in HAZ (Ref 19, 25).

It is imperative that understanding the relationship between microstructure, mechanical and corrosion properties of FSW in aluminum alloys, particularly in heat-treated aluminum alloys, is of significant technological and scientific interest. Moreover, there has not been any systematic study reporting the relationship between the welding parameters, especially in terms of energy, mechanical properties, and corrosion behavior. Thus, the aim of the work is to investigate how mechanical and corrosion properties can be related to microstructural changes controlled by the welding parameters in FSW AA 7475.

2. Experimental Materials

The chemical composition of the 7475 Al-alloy in as-rolled condition is given in Table 1.

2.1 Welding Parameters and Tool Specification

All butt joints were produced using a RM Series Friction Stir Welder Model RM1A-0.7. The machine can be operated with tool rotational speed up to 3000 rpm, axial load of 67 kN, and plunge rates from 0.1 to 1000 mm/min.

The axial force, torque, and penetration depth values could be recorded simultaneously during each welding operation with the help of load cell coupled with a DAQ system. All the butt welds were made under displacement control mode, i.e., the depth of penetration was kept constant but the axial force response and torque are not directly controlled. The tool used was made of steel SKD61 and composed of a shank, flat shoulder (diameter 32 mm), and threaded probe (diameter 10 mm) as shown in Fig. 1. The tool axis was tilted by 2° with respect to the vertical axis of the plate surface. Rotational speed was varied and travel speed was kept constant at 50 mm/min. The FSW parameters studied are listed in Table 2. The depth of probe tip from the upper surface of the aluminum plate was also kept constant at 8.65 mm.

2.2 Energy Calculation

Since in FSW process friction heats the material, which is then essentially extruded around the tool before being forged by the large down pressure (Ref 27), role of energy on microstructure and joint strength has been emphasized. The energy (Ref 28) for FSW was calculated using the following expressions and the energy values are summarized in Table 3.

$$\text{Energy} = \int_{t=0}^{t=\text{end of welding}} Cz(t) \times \frac{Np \times 2\pi}{60}\, dt \qquad \text{(Eq 1)}$$

where Cz and Np represent respective torque and rpm.

Table 1 Base metal composition (wt.%)

Element	Zn	Mg	Cu	Fe	Si	Mn
Base metal	6.07	2.28	1.69	0.16	0.12	0.050

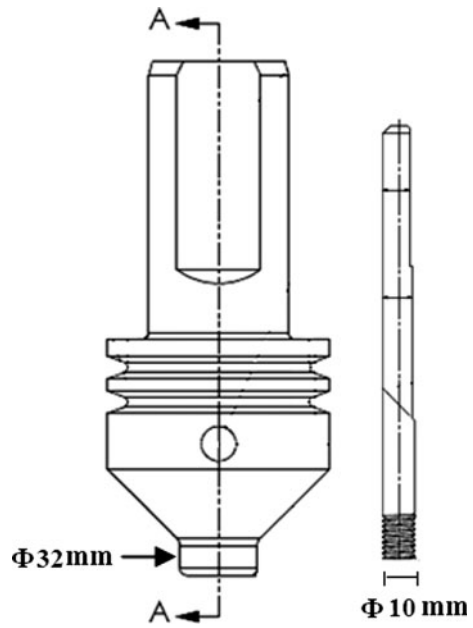

Fig. 1 Schematic diagram of tool and pin

2.3 Metallographic Study

The samples for metallographic studies were first cut and then polished using standard method and finally were etched with Keller's reagent [2 mL HF (48%) + 3 mL HCl + 5 mL HNO_3 + 190 mL distilled H_2O] to reveal the microstructure. Microstructural examination was carried out using a light optical microscope (Make: Carl ZEISS; Model: Imager.A1m) and the microphotographs were taken at different magnifications.

2.4 Microhardness Test

Microhardness measurements were performed on metallographically polished and etched samples across the butt joint from aluminum base metal through the different zones using Lica Vickers Micro Hardness Tester (Model: A-1170) at load 50 gf with dwell time 10 s and at an interval of 100 μm.

2.5 Tensile Strength Test

The welded joints were sliced in the transverse direction to make the tensile specimens as per ASTM E8M-04 shown in Fig. 2. The tensile test was performed on a Universal Testing Machine (INSTRON 8862) of 100 kN capacities at a cross head speed of 0.5 mm/min. The average fracture load values of four specimens were taken for each combination of parameters.

2.6 Corrosion Study

The area of base metal, SZ, and TMAZ individually as well as across the cross sections of four different weld metals are exposed to 3.5% NaCl solution for corrosion study. The potentiostatic polarization curves for base metal, SZ, and TMAZ as well as weld metals were determined in 3.5% NaCl solution using AUTOLAB PGSTAT 302 Potentiostatic machine at a scan rate of 0.5 mv/s. Ag/AgCl electrode was used as reference and platinum was used as counter electrode. Taffel's slopes were derived from the polarization curve.

2.7 SEM Study

Fracture surfaces of the tensile fractured specimens and the corroded samples were examined under JEOL JSM-8360 scanning electron microscope (SEM) to understand the mode of fracture.

Table 2 FSW parameters

Sl. no	Sample no.	Rotational speed, rpm	Traverse speed, mm/min
1	FR3	300	50
2	FR4	400	50
3	FR7	700	50
4	FR10	1000	50

Table 3 Energy of different FSW joints

Sl. no	Sample no.	Energy, kJ
1	FR3	57.2
2	FR4	59.2
3	FR7	62.6
4	FR10	87.2

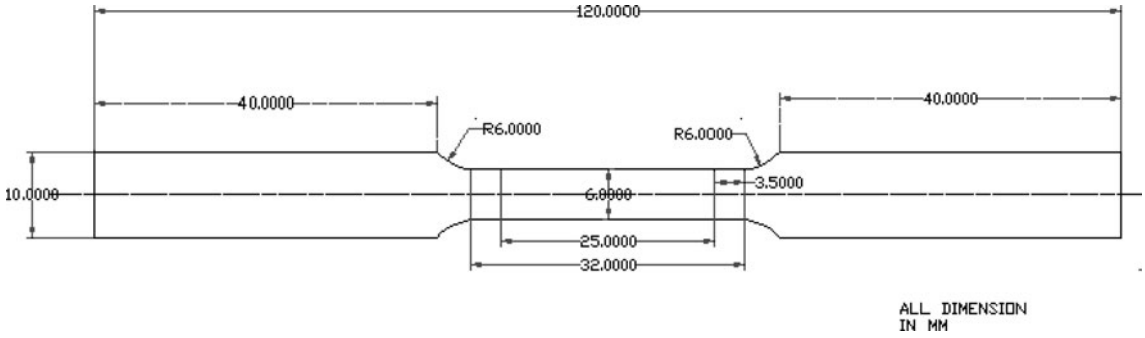

Fig. 2 Schematic diagram of tensile specimen (ASTM E8M-04)

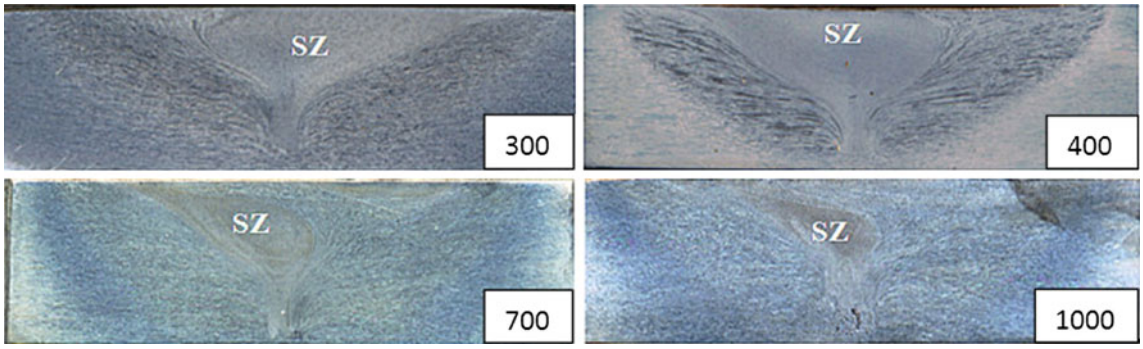

Fig. 3 Macrostructure of cross section of friction stir welded joint

3. Results and Discussion

3.1 Macrostructure

Typical cross section of the welded joints under different parameters is shown in Fig. 2. The formation of different zones in FSW such as stir zone (SZ), TMAZ, and HAZ are quite evident from the macrostructures. Depending on processing parameter, tool geometry, temperature of work piece, and thermal conductivity of the material, different shapes of SZ have been observed. Sato et al. (Ref 6) reported the formation of basin-shaped SZ on friction stir welding of 6063 Al-T5 plate. On the other hand, Rhodes et al. (Ref 3) and Mahoney et al. (Ref 29) reported elliptical SZ in the weld of 7075 Al-T6. In the present investigation, a change in shape of SZ on friction stir welding of 7475 Al-alloy from basin-shaped to elliptical shaped has been observed at higher tool rotation of ≥ 700 rpm (Fig. 3). Similar change in shape of SZ at higher tool rotation speed with the same tool geometry was reported by Mishra and co-workers (Ref 30). The area of SZ has been measured from macrographs using Autocad and the values are given in Table 3.

The area of stir zone has been tried to correlate with energy input as shown in Fig. 4. It is observed from Fig. 3 that with increasing tool rotation speed from 300 to 400 rpm, area fraction of the stir zone (SZ) first increases and with further increasing tool rotation speed from 400 to 1000 rpm, area fraction of the stir zone decreases (Table 4). In friction stir welding, metal flow and temperature play an important role in forming different zones in the welded joint. Formation of SZ, in particular, involves stirring which is related to flow of plasticized material. Material flow in the SZ is dominated by

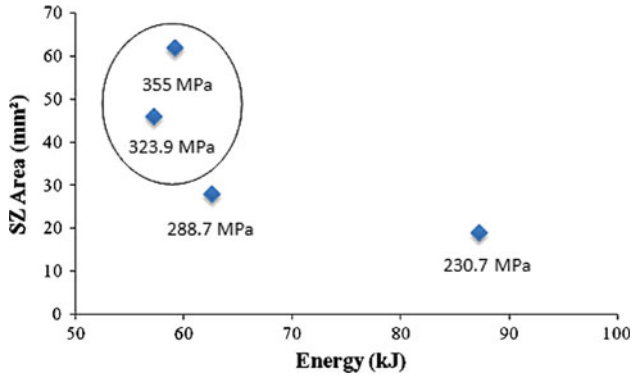

Fig. 4 Stir zone (SZ) area vs. energy input plot for different welded joints

the rotation of the pin. The material release from the pin surface through outward-spinning motions provides an intrinsic driving force for the downward spiral motion of the plasticized material along the pin. The SZ expands when the material immediately outside SZ could flow toward pin by following the SZ extremity and be forced directly into SZ. With increasing rpm more intense heating results in higher temperature. North et al. (Ref 31), Bjornekelett et al. (Ref 32), and Frigaared et al. (Ref 33) have suggested that eutectic melting of the material may occur at the tool interface. Such condition at the tool-material interface will decrease the torque which will ultimately decrease the outward-spinning motion. Thus, there should be an optimum energy where area of stirring will be maximum. In the present study, maximum area of stirring (62 mm^2) has been obtained at energy level of 59.2 kJ (Fig. 4).

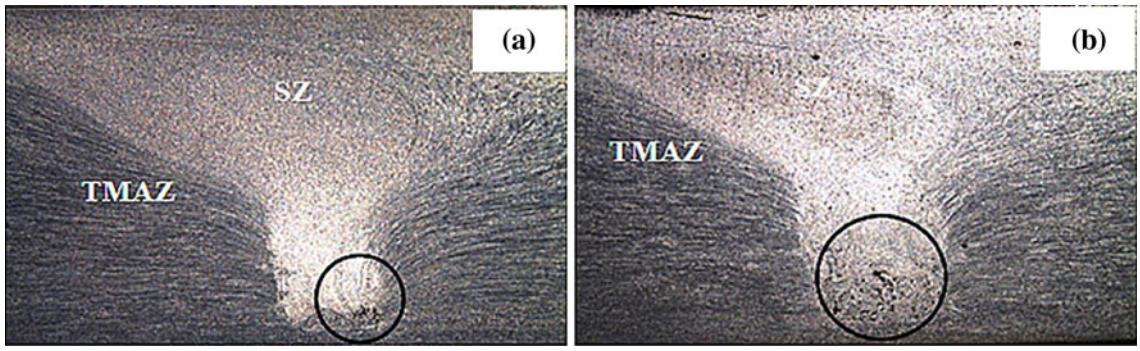

Fig. 5 Macrographs of voids at rpm 700 and 1000

Table 4 Area of stir zone measured from macrograph

Weld samples	FR3	FR4	FR7	FR10
SZ area, mm^2	46	62	28	19
Energy, kJ	57.2	59.2	62.6	87.2

Further, it is to be mentioned here that, some microvoids are observed at the bottom portion of the macrographs in welds of FR7 and FR10 (Fig. 5). FSW joints are prone to defects like pin hole, tunnel defect, piping defect, cracks, etc. due to improper flow of metal and insufficient consolidation of metal in the weld region. Olga (Ref 34) reported that in FSW, as the rotational speed increases, the heat input also increases resulting in more intense stirring and mixing of materials. Higher tool rotational speed associated with higher heat generation (energy) leads to the excessive release of stirred material to the upper surface, which resultantly produced microvoids in the stir zone. Interestingly, the two welds (FR7 and FR10) which show microvoids (Fig. 5) are involved with relatively higher energy (Table 3).

3.2 Microstructure

The microstructure of base metal (AA7475 aluminum alloy) as given in Fig. 6 shows α-aluminum and some particles (precipitates). Again the grains are observed to be elongated. Figures 7 to 9 show the optical micrographs of SZ, TMAZ, and HAZ of all the FSW joints performed under different combinations of FSW parameters.

The stir zone (Fig. 7) consists of fine equiaxed grains due to dynamic recrystallization. Adjacent to the stir zone, the TMAZ (Fig. 8) region shows the severe deformation of grains due to the stirring action of the tool pin. It is evident that the welding parameters, especially rotation speed, affected the grain size in the stir zone of weld. At a given travel speed, an increase in rotation speed the grain size increases (Fig. 7a to d). This is due to the effect of heat input and it is well known that grain size increases with increasing heat input. The HAZ (Fig. 9) shows relatively finer grain than base metal. However, the elongated grains characteristic of the rolled base plate still exist. Furthermore, for both TMAZ and HAZ, grain size increases with increase in rotational speed. At a particular rpm grain coarsening is significantly observed from stir zone to TMAZ and HAZ. This is applicable for all the four parameters studied. In TMAZ region, the FSW tool has plastically deformed the material without recrystallization and the heat from the adjacent

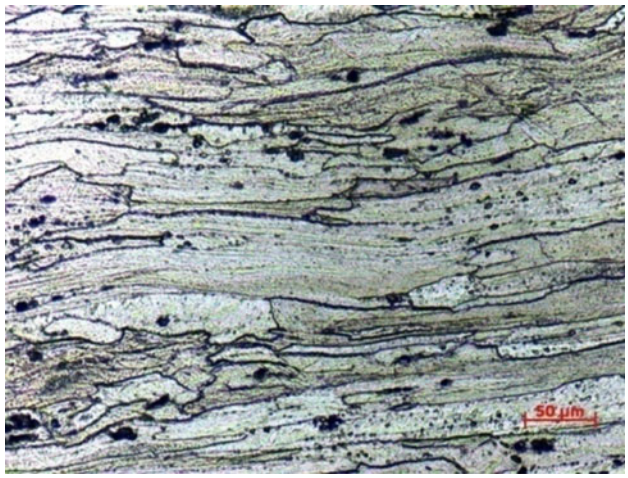

Fig. 6 Microstructure of base metal

zone has resulted coarser grain size compared to stir zone. The HAZ region is basically base metal affected by a thermal cycle only and hence the original microstructure of the base metal has been modified though the characteristic elongated grains of the rolled base plate still exists. Furthermore, it is likely that $MgZn_2$ particles could be present in the structure as all binary intermetallic phases are assumed to have negligible ternary (Al-Mg-Zn) solubility except for $MgZn_2$. Again, the composition of the base metal falls into the region of (Al) + $MgZn_2$ as can be seen from pseudo-binary diagram (Fig. 10) of Al-Mg-Zn at 5.33% Zn (Ref 35).

3.3 Microhardness Test

Microhardness was measured across the mid-thickness region of the weld as shown schematically in Fig. 11. The distribution of hardness values across the welded joint is presented in Fig. 12. It is observed from Fig. 12 that the hardness values gradually increased from the base metal and reached maximum at SZ and then decreased to the base metal region irrespective of the tool rotational speed used (Ref 36). Maximum hardness at each point is observed in weld FR4; whereas minimum hardness at each point is associated with weld FR10. Among the three different zones (SZ, TMAZ, and HAZ), maximum hardness is achieved in SZ which is attributed due to finer grain size. For TMAZ, which has experienced plastic deformation, significant grain coarsening has caused lower hardness than SZ. The hardness of HAZ is still lower

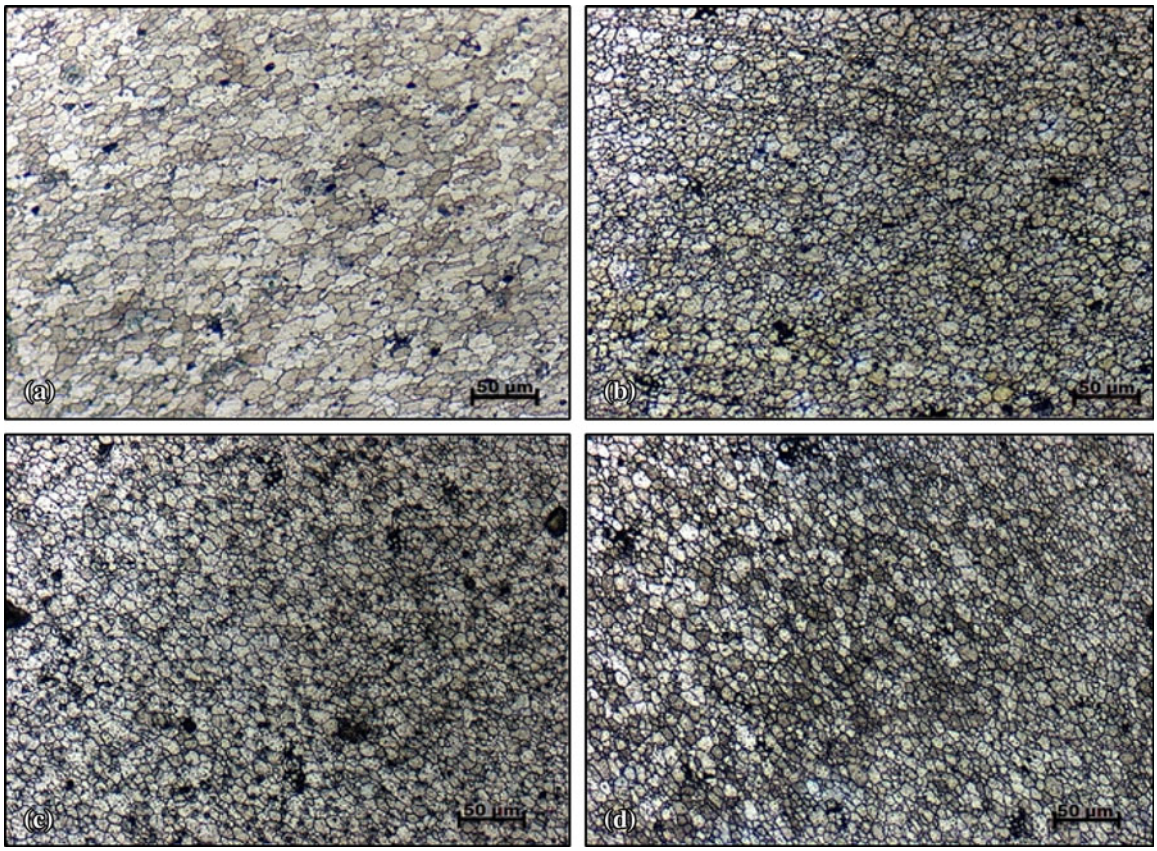

Fig. 7 Microstructure of SZ. (a) rpm 300, (b) rpm 400, (c) rpm 700, and (d) rpm 1000

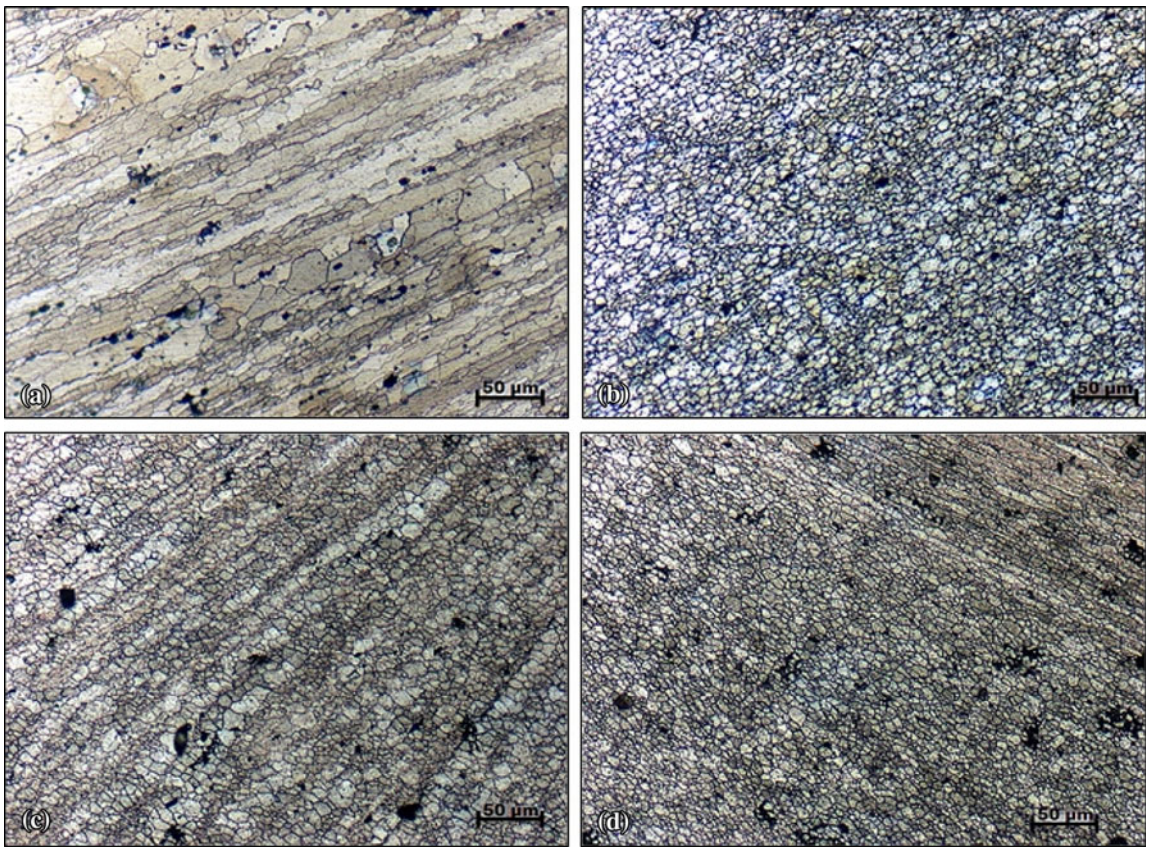

Fig. 8 Microstructure of TMAZ. (a) rpm 300, (b) rpm 400, (c) rpm 700, and (d) rpm 1000

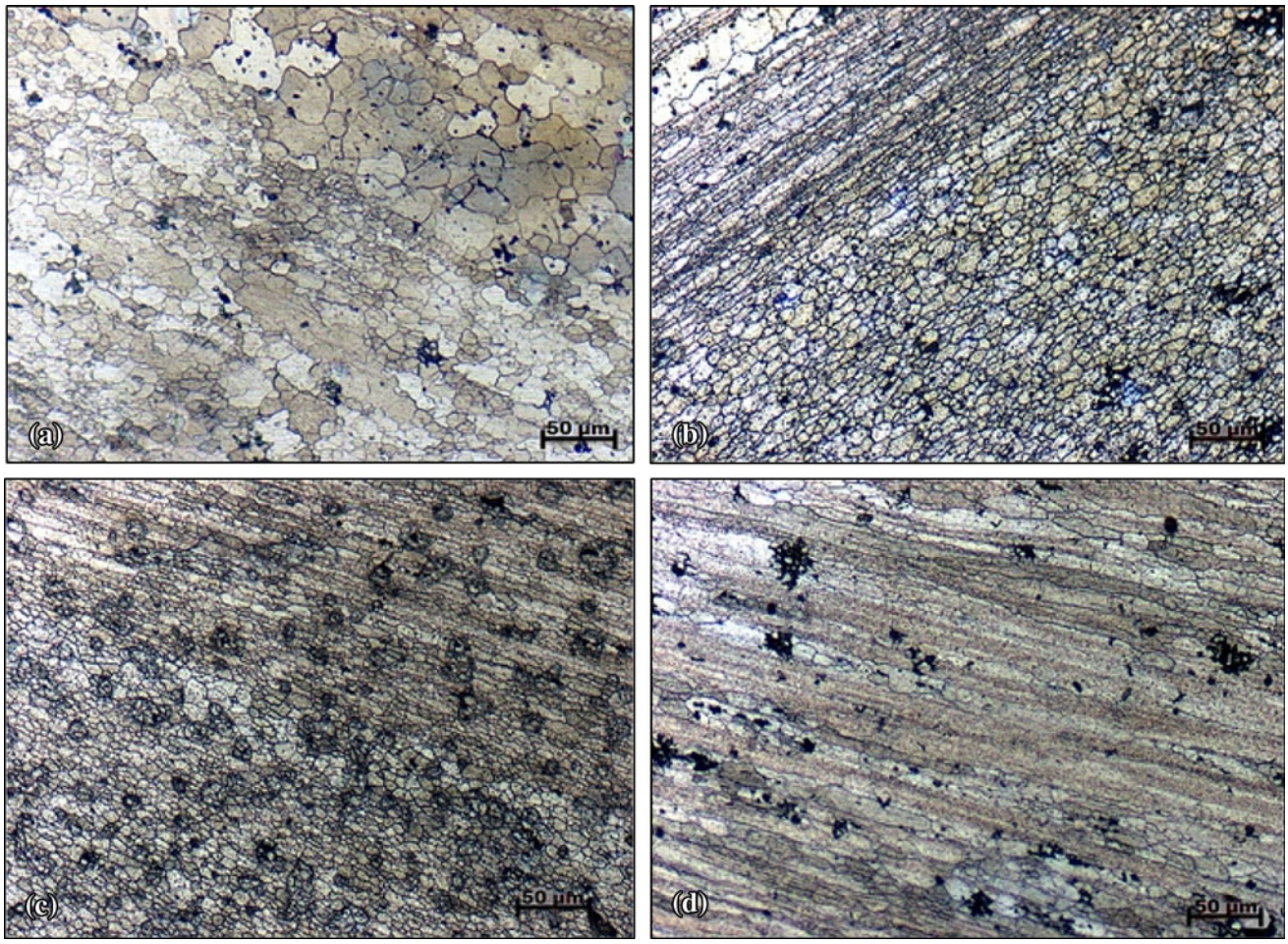

Fig. 9 Microstructure of heat-affected zone (HAZ). (a) rpm 300, (b) rpm 400, (c) rpm 700, and (d) rpm 1000

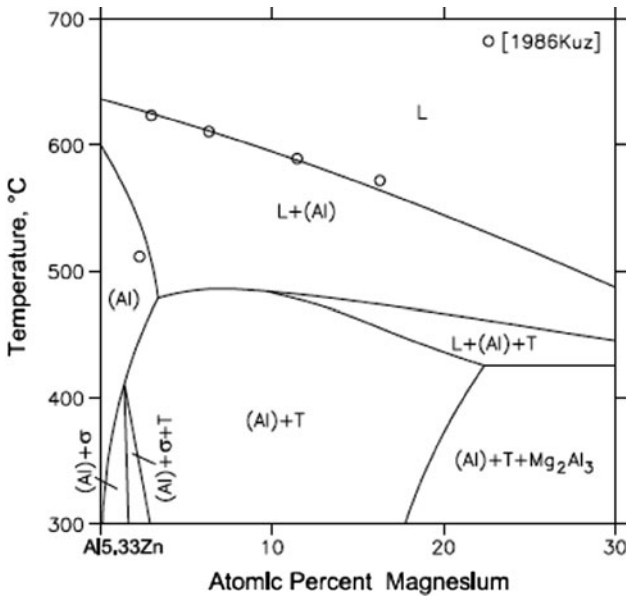

Fig. 10 Al-Mg-Zn compound vertical section at 5.33 at. %Zn (Ref 32)

than TMAZ. Basically this zone is affected by thermal cycle only resulting in alteration of base metal microstructure. Slight increase in hardness compared to base metal indicates no major change in microstructure (Fig. 10) has occurred. Thus it can be concluded that grain size exerted maximum effect on microhardness across the welded joints.

3.4 Tensile Strength Test

Tensile testing was performed for base metal and all four FSW joints. The tensile testing results of BM and FSW joints are given in Table 5.

Among the four FSW parameters studied, i.e., at 300, 400, 700, and 1000 rpm, the maximum tensile strength of FSW joint was achieved with rotational speed of 400 rpm and traverse speed of 50 mm/min. This variation of tensile strength with rotational speeds for a given traverse speed appears to be linked to the energy of the welds. It is apparent from Fig. 4 that improved joint strength could be achieved within a certain range of energy as marked through circle in the Fig. 4. Joint efficiency as high as 89.5% of base metal could be achieved at 400 rpm. Again, the joint strength values are consistent with the hardness profile shown in Fig. 12. The harder interface zone has yielded higher strength (rpm 400)

Fig. 11 Schematic diagram for microhardness traverse position

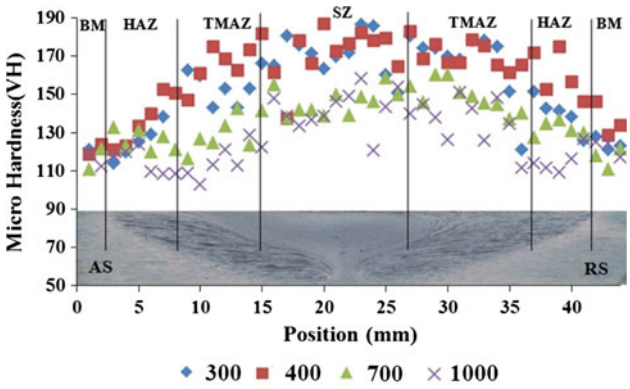

Fig. 12 Microhardness from AS to RS direction along the cross section of weld

Table 5 Tensile test results and joint efficiency of different weld joints

Sl. no.	Sample no.	Yield strength, MPa	Ultimate tensile strength, MPa	% Elongation	Joint efficiency, %
1	BM	268	397.01	16.56	
2	FR3	240.11	323.88	4.23	81.57
3	FR4	260.47	355	6.04	89.5
4	FR7	245.66	288	2.61	72.75
5	FR10	223.29	230	1.78	57.94

and relatively softer interface zone shows lower joint strength (rpm 1000).

Interestingly, all the FSW joints tensile fracture occurred at or near the interface between stir zone and TMAZ on the advancing side of the joint as shown in Fig. 13. Similar fracture location after tensile testing of FSW aluminum alloys was also reported by Liu et al. (Ref 37). The remarkable difference in the structure particularly grain size between SZ and TMAZ cause the fracture at or near the interface between the weld nugget and the TMAZ on the advancing side.

3.5 Tensile Fracture Surface Study Under SEM

The broken tensile samples were studied under SEM and the fractographs of samples are presented in Fig. 14. Fractographic examinations of the broken tensile samples from FSW joints reveal roughened fractures containing features having dimensions similar to the grain size of the SZ (Fig. 14a). The more ductile behavior is distinguished by the presence of numerous tear ridges (Ref 29). These ridges reflect the material's ability to sustain the tensile load after microvoid coalescence has begun;

Fig. 13 Location of fracture (from boundary of SZ and TMAZ) after tensile testing

absence of the ridges (Fig. 14c) indicates that the specimen fails soon after microvoid coalescence begins (Ref 29). The fracture surfaces of both conditions exhibit very fine microvoids on the exposed grain surfaces (Fig. 14b, d). Furthermore, there is a significant breakup of $MgZn_2$ particles, subsequently creating a uniform distribution of finer $MgZn_2$ particles in the α-aluminum matrix of optimized FSW parameters. However, regardless of welding parameters, some particle coarsening and clustering were observed in the vicinity of the tensile fractured area of friction stir welded specimen (Ref 36).

3.6 Corrosion Study of Base Metal and Different Welded Joints

Potentiostatic polarization study has been done for base metal and SZ, TMAZ individually in each of the four different weld metals and across the cross sections of four different weld metals in 3.5% NaCl solution. From the potentiostatic polarization study corrosion rate and E_{corr} have been evaluated and are given in Table 6. Corrosion resistance property for both SZ and TMAZ increases as the rpm increases. When comparing the corrosion rate between SZ and TMAZ in a given welded joint, TMAZ shows a poor corrosion resistance as compared to SZ. Furthermore, corrosion rate across the cross sections of four different weld metals shows similar trend with individual zone, i.e., the corrosion resistance property also increases with increasing rpm.

The reactivity of the welds is influenced by the welding parameter such as rotation speed. Precipitates start to occur at the grain boundaries due to higher nucleation rate at the grain boundaries (Ref 38-44). An increase in rotational speed, increases grain size and also likely to increase more precipitates. From Table 6 it is observed that the reactivity in the SZ decreases with increasing rotation speed. It is likely that the high rotation speed leads to a high temperature, maximizing dissolution of precipitate particles, and the cooling rate helps to retain the solutes in solid solution (Ref 45). Also, more uniform solute distribution is expected from the higher temperatures experienced in the SZ.

On the other hand, TMAZ heats up to a temperature just below the solutionizing temperature of the alloy (Ref 46). This results in coarsening of precipitates, as evident from the decrease in the hardness (Fig. 10). Again, an increase in

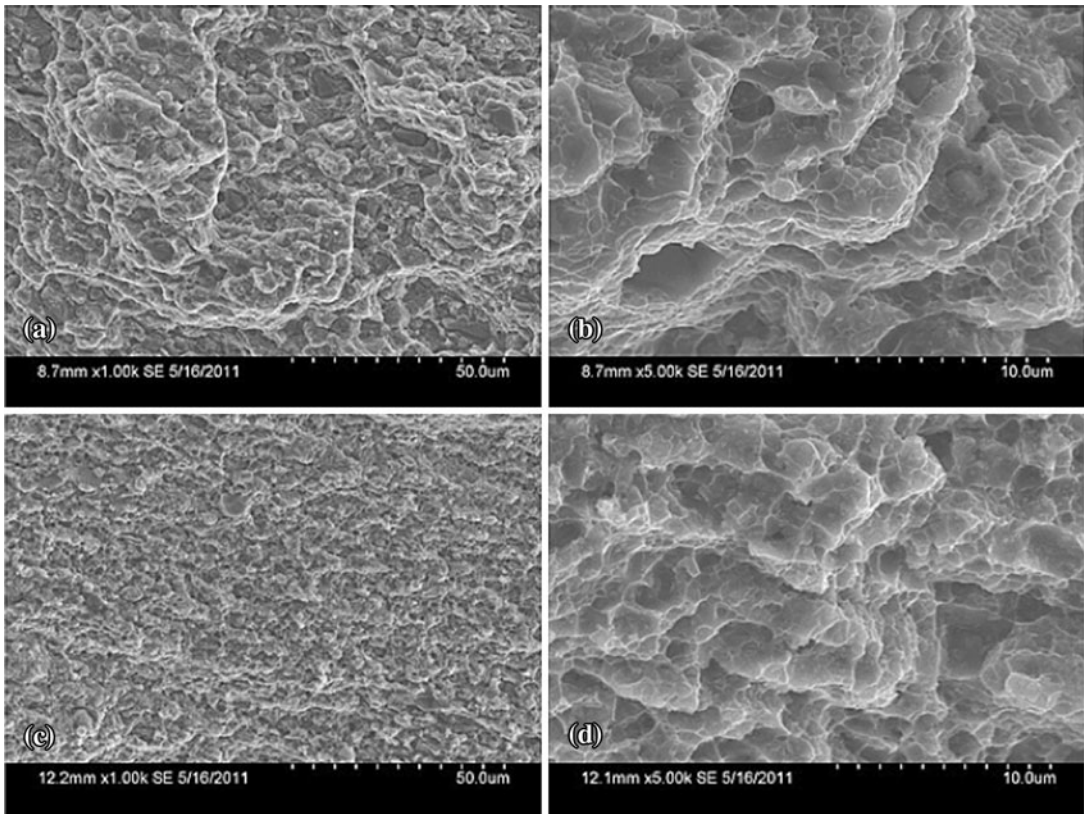

Fig. 14 Fracture surface of tensile samples (a) rpm 400 at magnification 1.00K×, (b) rpm 400 at magnification 5.00K×, (c) rpm 1000 at magnification 1.00K×, and (d) rpm 1000 at magnification 5.00K×

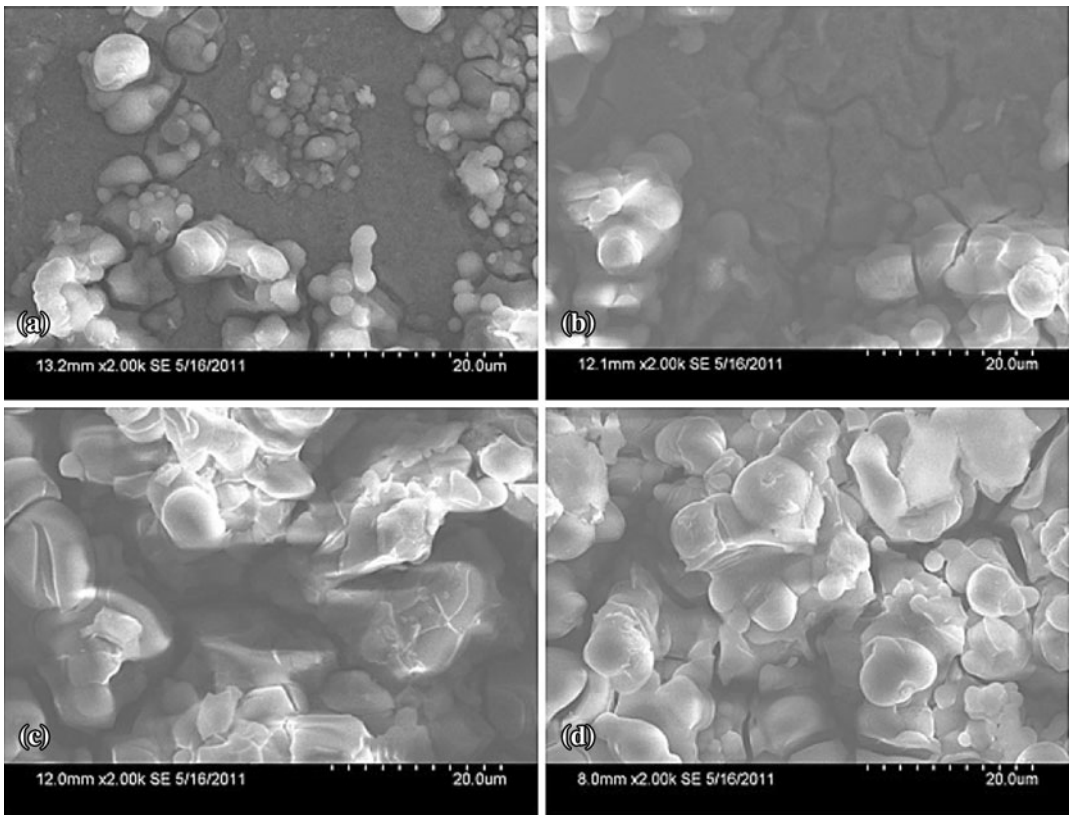

Fig. 15 SEM micrograph of SZ (a, b) and TMAZ (c, d) after corrosion test

Table 6 Corrosion rate for welded joints

Sample	Corrosion rate, mm/year	E_{corr}, V
Base metal	1.2	−0.694

	SZ		TMAZ		Full surface	
Sample	Corrosion rate, mm/year	E_{corr}, V	Corrosion rate, mm/year	E_{corr}, V	Corrosion rate, mm/year	E_{corr}, V
FR3	1.152	−0.685	3.31	−0.705	1.59	−0.835
FR4	0.906	−0.678	3.01	−0.672	1.05	−0.764
FR7	0.901	−0.667	2.95	−0.661	0.99	−0.751
FR10	0.895	−0.657	1.44	−0.652	0.95	−0.733

rotational speed, increases grain size. With increase in grain size, precipitation now starts to occur in a matrix due to lower grain boundary area. This probably increases the potential between matrix and grain boundary area, making corrosion attack more favorable.

The slightly more negative critical potential of TMAZ than SZ for all the four parameters can be attributed to the residual stresses induced during the process of FSW. Hence it can be concluded that corrosion resistance of SZ is better than that of TMAZ. However, there exists a problem of galvanic kind of corrosion because of difference in potentials across the friction welded joint, especially in aggressive environments containing halide ions (Ref 46).

3.7 SEM Micrographs of Corroded Surfaces

Corroded samples after potentiostatic polarization study have been examined under SEM and the SEM micrographs of different zones (SZ and TMAZ) are shown in Fig. 14.

The corrosion morphology of the welds shows presence of intergranular attack along with some pits in both SZ and TMAZ regions (Fig. 15). This is consistent with the higher reactivity for TMAZ than SZ.

4. Conclusion

- Butt joint of 9 mm 7475 aluminum alloy (9 mm) could be successfully made by the FSW process and joint efficiency as high as 89.5% of base metal could be achieved.
- The maximum tensile strength of FSW joint was achieved with rotational speed of 400 rpm and traverse speed of 50 mm/min. The variation of tensile strength with rotational speeds is well linked with the energy of the welds. Improved joint strength could be achieved within a certain range of energy, i.e., 57.2 and 59.2 kJ.
- The maximum tensile strength of FSW joint corresponds to maximum area of stirring (62 mm^2) which attributed maximum grain refinement and maximum hardness.
- As evaluated from potentiostatic polarization studies the corrosion resistance property for both SZ and TMAZ increases with increasing rpm from 300 to 1000. In other words, maximum corrosion resistance property of welds was obtained at rotational speed of 1000 rpm and traverse speed of 50 mm/min. However, for a given welded joint, SZ shows better corrosion resistance compared to TMAZ.

References

1. M. Thomas, E.D. Nicholas, J.C. Needham, M.G. Murch, P. Temple-Smith, and C.J. Dawes, Friction Welding, The Welding Institute, United States Patent, 460,317, Cambridge, GB, 1995
2. J.Q. Su, T.W. Nelson, R. Mishra, and M. Mahoney, Microstructural Investigation of Friction Stir Welded 7050-T651 alloy, *Acta Mater.*, 2003, **51**, p 713–729
3. C.G. Rhodes, M.W. Mahoney, W.H. Bingel, R.A. Spurling, and C.C. Bampton, Effects of Friction Stir Welding on Microstructure of 7075 Aluminum, *Scripta Mater.*, 1997, **36**, p 69–75
4. K.V. Jata, K.K. Sankaran, and J.J. Ruschau, *Metall. Mater. Trans. A*, 2000, **31A**, p 2181–2192
5. G. Liu, L.E. Murr, C.-S. Niou, J.C. McClure, and F.R. Vega, Microstructural Aspects of the Friction Stir Welding of 6061-T6 Aluminum, *Scripta Mater.*, 1997, **37**, p 355–361
6. Y.S. Sato, H. Kokawa, M. Enomoto, S. Jogan, and T. Hashimoto, Precipitation Sequence in Friction Stir Weld of 6063 Aluminum During Aging, *Metall. Mater. Trans. A*, 1999, **30A**, p 3125–3130
7. Y.S. Sato, H. Kokawa, M. Enomoto, and S. Jogan, *Metall. Mater. Trans. A*, 1999, **30A**, p 2429–2437
8. K.V. Jata and S.L. Semiatin, Continuous Dynamic Recrystallization During Friction Stir Welding of High Strength Aluminium Alloys, *Scripta Mater.*, 2000, **43**, p 743–749
9. S. Benavides, Y. Li, L.E. Murr, D. Brown, and J.C. McClure, Low-Temperature Friction-Stir Welding of 2024 Aluminum, *Scripta Mater.*, 1999, **41**, p 809–815
10. M. Peel, A. Steuwer, M. Preuss, and P.J. Withers, Microstructure, Mechanical Properties and Residual Stresses as a Function of Welding Speed in Aluminium AA5083 Friction Stir Welds, *Acta Mater.*, 2003, **51**, p 4791–4801
11. A.P. Reynolds, W.D. Lockwood, and T.U. Seidel, Processing-Property Correlation in Friction Stir Welds, *Mater. Sci. Forum*, 2000, **331–337**, p 1719–1724
12. H.J. Liu, H. Fujii, M. Maeda, and K. Nogi, Tensile Properties and Fracture Locations of Friction-Stir-Welded Joints of 2017-T351 Aluminum Alloy, *J. Mater. Process. Technol.*, 2003, **142**, p 692–696
13. B. Yang, J. Yan, M.A. Sutton, and A.P. Reynolds, Banded Microstructure in AA2024-T351 and AA2524-T351 Aluminum Friction Stir Welds Part I. Metallurgical Studies, *Mater. Sci. Eng. A*, 2004, **364**, p 55–65
14. K.A.A. Hassan, A.F. Norman, and P.B. Prangnell, *Mater. Sci. Forum*, 2002, **396–402**, p 1549–1554
15. K.V. Jata, Friction Stir Welding of High Strength Aluminium Alloys, *Mater. Sci. Forum*, 2000, **331–337**, p 1701–1712
16. K.A.A. Hassan, A.F. Norman, D.A. Price, and P.B. Prangnell, *Acta Mater.*, 2003, **51**, p 1923–1936
17. K. Elangovan and V. Balasubramanian, Influences of Pin Profile and Rotational Speed of the Tool on the Formation of Friction Stir Processing Zone in AA2219 Aluminium Alloy, *Mater. Sci. Eng. A*, 2007, **459**, p 7–18
18. J.B. Lumsden, M.W. Mahoney, C.G. Rhodes, and G.A. Pollock, Corrosion Behavior of FSW 7050-T7651, *Corrosion*, 2003, **59**, p 212–219

19. J.B. Lumsden, M.W. Mahoney, G. Pollock, and C.G. Rhodes, Intergrannular Corrosion Following Friction Stir Welding of Aluminium Alloy 7075-T651, *Corrosion*, 1999, **55**, p 1127–1135
20. C.S. Paglia, M.C. Carroll, B.C. Pitts, A.P. Reynolds, and R.G. Buchheit, *Mater. Sci. Forum*, 2002, **396–402**, p 1677–1684
21. W. Hu and E.I. Meletis, Corrosion and Environment-Assisted Cracking Behavior of Friction Stir Welded Al2195 and Al2219 Alloys, *Mater. Sci. Forum*, 2000, **331–337**, p 1683–1688
22. G.S. Frankel and Z. Xia, Localized Corrosion and Stress Corrosion Cracking Resistance of Friction Stir Welded Al Alloy 5454, *Corrosion*, 1999, **55**, p 139–150
23. J. Corral, E.A. Trillo, Y. Li, and L.E. Murr, Corrosion of Friction-Stir Welded Aluminum Alloys 2024 and 2195, *J. Mater. Sci. Lett.*, 2000, **19**, p 2117–2122
24. F. Zucchi, G. Trabanelli, and V. Grassi, Pitting and Stress Corrosion Cracking Resistance of Friction Stir Welded AA 5083, *Mater. Corros.*, 2001, **52**, p 853–859
25. A. Squillace, A.D. Fenzo, G. Giorleo, and F. Bellucci, A Comparison Between FSW and TIG Welding Techniques: Modifications of Microstructure and Pitting Corrosion Resistance in AA 2024-T3 Butt Joints, *J. Mater. Process. Technol.*, 2004, **152**, p 97–105
26. S. Williams, R. Ambat, D. Price, M. Jariyaboon, A. Davenport, and A. Wescott, *Mater. Sci. Forum*, 2003, **426–432**, p 2855–2860
27. M.J. Pee, A. Steuwer, P.J. Withers, T. Dickerson, Q. Shi, and H. Shercliff, *Metall. Mater. Trans. A*, 2006, **37A**, p 2183–2193
28. Z. Sandra, L. Laurent, L. Julien, and B. Régis, Experimental Investigation of the Influence of the FSW Plunge Processing Parameters on the Maximum Generated Force and Torque, *Int. J. Adv. Manuf. Technol.*, 2010, **47**, p 201–215
29. M.W. Mahoney, C.G. Rhodes, J.G. Flintoff, R.A. Spurling, and W.H. Bingel, *Metall. Mater. Trans. A*, 1998, **29**, p 1955
30. Z.Y. Ma, R.S. Mishra, and M.W. Mahoney, *Friction Stir Welding and Processing II*, K.V. Jata, M.W. Mahoney, R.S. Mishra, S.L. Semiatin, and T. Lienert, Ed., TMS, San Diego, 2003, p 221–230
31. T.H. North, G.J. Bendzsak, and C. Smith, Material Properties Relevant to FSW Modellimg, *2nd International Conference on Friction Stir Welding*, Gothenburg, Sweden, 2000
32. B.L. Bjornklett, O. Frigaard, O. Grong, O.R. Myhr, and O.T. Midling, Modelling of Local Melting During Friction Stir Welding of Al-Zn-Mg alloys, *ICAA-6:6th International Conference on Aluminium Alloys*, Japan, 1998
33. O. Frigaard, O. Grong, B. Bjornklett, and O.T. Midling, Modeling of the Thermal and Microstructure Fields During Friction Stir Welding of Aluminium Alloys, *1st International Symposium on Friction Stir Welding*, Thousand Oaks, CA, June 1999
34. V.F. Olga, Microstructural Issues in a Friction-Stir-Welded Aluminum Alloy, *Scripta Mater.*, 1998, **38**(5), p 8–703
35. H. Liang, S.L. Chen, and Y.A. Chang, A Thermodynamic Description of the Al-Mg-Zn System, *Metall. Mater.Trans. A*, 1997, **28A**, p 1725–1734
36. M. Jayaraman, R. Sivasubramanian, and V. Balasubramanian, Establishing Relationship Between the Base Metal Properties and Friction Stir Welding Process Parameters of Cast Aluminium Alloys, *Mater. Des.*, 2010, **31**, p 4567–4576
37. H.J. Liu, H. Fujii, M. Maeda, and K. Nogi, Tensile Properties and Fracture Locations of Friction-Stir-Welded Joints of 2017-T351 Aluminum Alloy, *J. Mater. Process. Technol.*, 2003, **142**, p 692–696
38. H.-C. Shih, N.-J. Ho, and J.C. Huang, Kinetic Study of Precipitation Behavior in Al-Cu-Mg and 2024 Aluminum Alloys, *Metall. Mater. Trans. A*, 1996, **27A**, p 2479–2494
39. C.R. Brooks, *Heat Treatment, Structure and Properties of Nonferrous Alloys*, ASM, Metal Park, OH, 1982
40. M. Rosen, E. Horowitz, L. Swartzendruber, S. Fick, and R. Mehrabian, *Mater. Sci. Eng.*, 1982, **53**, p 191–198
41. S.G. Mazzini and J.C. Caretti, *Scripta Metall. Mater.*, 1991, **25**, p 1987–1990
42. J.M. Silcock, *J. Inst. Met.*, (1960–1961), **89**, p 203–210
43. R.E. Reed-Hill, *Physical Metallurgy Principles, D*, Van Nostrand Company Inc., Toronto, 1964
44. M. Van Lancker, *Metallurgy of Aluminium Alloys*, Chapman & Hall, London, 1967
45. K.A.A. Hassan, P.B. Prangnell, A.F. Norman, D.A. Price, and S.W. Williams, *Sci. Technol. Weld. Join.*, 2003, **8**, p 257–268
46. T. Venugopal, K. Srinivasa Rao, and K. Prasad Rao, Studies on Friction Stir Welded AA 7075 Aluminum Alloy, *Trans. Indian Inst. Met.*, 2004, **57**(6), p 659–663